POLITECNICO DI TORINO
Repository ISTITUZIONALE

Strength and ductility of confined concrete columns under axial load and biaxial bending

Original
Strength and ductility of confined concrete columns under axial load and biaxial bending / Colajanni, P., Fossetti, M., Cavaleri, L., DI TRAPANI, F., Macaluso, G., Papia, M.. - ELETTRONICO. - (2012). (World Conference on Earthquake Engineering Lisbona 24-28 settembre 2012).

Availability:
This version is available at: 11583/2672000 since: 2017-05-25T22:40:50Z

Publisher:
Sociedade Portuguesa de Engenharia Sismica (SPES)

Published
DOI:

Terms of use:

This article is made available under terms and conditions as specified in the corresponding bibliographic description in the repository

Publisher copyright

(Article begins on next page)

18 November 2026

Strength and Ductility of Confined Concrete Columns under Axial Load and Biaxial Bending

P. Colajanni
University of Messina, Italy

M. Fossetti
University of Enna, Italy

L. Cavaleri, F. Di Trapani, G. Macaluso, M. Papia
University of Palermo, Italy

SUMMARY:
The behaviour of prismatic reinforced concrete columns under increasing eccentric compression load was experimentally investigated and analytically modelled. Columns with distributed longitudinal reinforcement and closely spaced transverse reinforcement were tested up to failure, considering different values and directions of eccentricity. Preliminary tests were carried out under concentric compression in order to validate the choice of the stress-strain laws adopted for the confined concrete and the longitudinal steel bars in compression. In the paper, closed form expressions able to approximate the experimental results in the case of uniaxial bending are presented. Finally, a fibre numerical model is utilized for the cases of biaxial bending. The results show the reliability of the analytical models and suggest further studies to relate analytically the components of ultimate bending moment and curvature, in the cases of biaxial bending, to the values corresponding to two separate cases of uniaxial bending under the same level of compression.

Keywords: Confined concrete, Biaxial bending, Analytical model, Experimental tests

1. INTRODUCTION

The seismic response and the capacity of Reinforced Concrete (RC) frames are strictly dependent on the strength and available ultimate rotation of the plastic hinges activated in global collapse mechanisms. Once the brittle failure of the beam to column joints and the shear collapse of beams and columns are avoided, structure collapse is often governed by the rotation capacity of the plastic hinges at the ends of the columns: the more they are reduced, the greater the compression levels are.
This phenomenon governs the seismic behavior of both newly designed frames, where the region at the base of the columns of the first storey is adequately involved by the designed global collapse mechanism, and existing structures, where generally a soft storey mechanism is activated. Thus in both cases the structure's seismic capacity is proportional to the available plastic rotation of the plastic hinges at the top and base of the storey columns involved in the collapse mechanism.
Exact analytical evaluation of strength and rotation capacity of reinforced concrete sections subjected to axial force and biaxial bending is made difficult by the following occurrences:- the flexure axis is not coincident with a principal inertia axis of the section; - the evaluation of the plastic rotation capacity requires assumption of suitable constitutive stress-strain relationships for steel and concrete, able to take into account the confinement effect on the concrete and the post-buckling behavior of the longitudinal steel rebars; - rigorous modelling of the effects of the cyclic actions.
It is noteworthy that in order to assess the ultimate strength of the section, the use of a simplified model (such as a rectangular or parabolic-rectangular stress-block) suggested by the international codes (ACI 318 – 2008, Eurocode 2) is justified by the fact that they include safety factors that lead to conservative evaluation of the section strength. By contrast, the assessment of plastic rotational capacity requires the adoption of more rigorous models of the behavior of the section in which the ultimate curvature is dependent on the axial force and the direction of the flexure axis.
Even if the analysis is limited to rectangular sections with uniformly distributed reinforcing bars placed symmetrically with respect to the principal axes of the section, the analytical models and the experimental investigations available in the literature are few.

The most common approach utilized for evaluation of section strength and rotation capacity for an assigned level of axial action is based on use of the classical fibre model proposed by Mari and Scordelis (1973) for discretization of the compressed part of the concrete section. Moreover, analytical models based on suitable strategies for stress integration in the compressed region have been derived (Bonet *et al*. 2001, Fafitis, 2001) and more general numerical procedures able to provide by iterative approach the three-dimensional strength domain in the *N-Mx-My* space have been formulated (Di Ludovico *et al*., 2010) for sections of any shape.
Among the simplified analytical approaches suitable for practical applications able to derive the failure surface formerly defined by Bresler (1960), those by Bonet *et al*. (2004) and Monti and Alessandri (2006) are noteworthy; however, in this context many other solution procedures are available.
The experimental investigations in this field are few, due to the complexity of performing displacement-controlled tests on large-scale specimens. Moreover, the large number of the mechanical parameters that rule the response limit the generalization of the deduced statement. The results of monotonic and cyclic tests on square sections are reported in Zahn *et al.* (1989) and Bahn and Hsu (2000); results of many series of monotonic tests on rectangular and square sections are shown in Ramamurthy (1966).
The significance of the results presented here concerns both the analytical modelling and the experimental investigations. With respect to the former topic, closed form solutions for ultimate bending moments and ultimate and yielding curvatures are provided for rectangular reinforced concrete sections subjected to axial force and uni-axial moment. The formulation takes into account the effect of distributed secondary reinforcing bars, hardening of steel and confinement action on the concrete. With reference to the experimental tests, the former results of an ongoing research are reported that refers to 8 columns with a rectangular section subjected to axial action without eccentricity or with constant eccentricity in one or two directions.
The modelling of the test under axial force and biaxial bending is performed by a classic fibre model. The results show that the choice of the adopted stress-strain relationship for the confined concrete is so reliable that an accurate prediction of the experimental response can be derived.

2. TEST SPECIMENS AND SETUP

Eight tests were performed on nominally equal specimens, cast according to the structural scheme shown in Fig.1.1. In the regions close to the top and the base of the column, the stirrup and tie spacing is 50 mm; in the central region, where specimen collapse is expected, the spacing is 80 mm. The parts at the top and base of the specimen with a larger cross-section were designed in such a way as to place the devices allowing rotations at the specimen ends when an eccentric load was applied. Nevertheless, eccentricities were always internal to the cross-section of the central region of the specimen.
The values of unconfined concrete strength, peak and ultimate deformations (the latter corresponding to a strength reduction with respect to the peak strength of 15%) were deduced as the mean values of the results of experimental tests on cylindrical specimens with diameter 150 mm and height 300 mm,

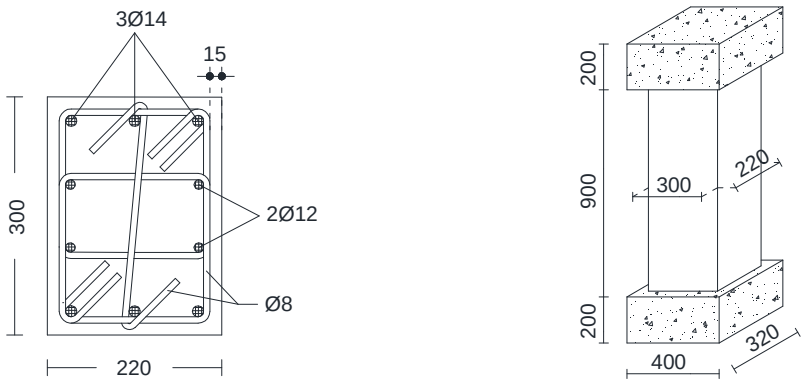

Figure 1.1. Structural scheme of specimens (dimensions in mm)

and were are equal to f_{co}=24.63 MPa, ε_{co}=0.002, ε_{co85}=0.0028. Stirrups, ties and longitudinal reinforcement were made with B450C steel with a yield stress value equal to 450 MPa (fy=450 MPa).
Fig.2.1 shows the disposition of reinforcement before specimen casting, a cast specimen and a test phase. A press with 4000 kN load carrying capacity was used to test all the specimens in a displacement-controlled mode. The data acquisition program of the test machine shows the force-displacement or force-deformation curve in real time, allowing the operator to stop the test if anomalous behaviour is detected. The deformation was recorded by four gauges with precision 1/1000 mm suitably placed on the four sides of the specimen, depending on the eccentricity of the applied load. Four more gauges were placed on the internal face of the larger parts at the ends of the specimen, with gauge length 900 mm.
Since tests were performed up to collapse, when heavy damage on the specimen occurred, the gauges on the side of the specimen were removed, due to the loss of the ability to detect the displacement and in order to prevent the instruments from being damaged. The other four gauges, placed on the internal face of the large parts at the ends of the specimens, recorded the response up to the end of the test.
When an eccentric axial load was applied, between the bases of the specimens and the plate of the test machine devices were placed to enable rotation of the specimens. The devices were made up of steel plates with cylindrical rabbets containing a suitably lubricated steel cylinder. A picture of these devices will be shown below.

Figure 2.1. Arrangement of reinforcement, specimen and specimen under test

3. CONCENTRIC COMPRESSION AND MODELLING OF MATERIALS

Two specimens, namely CC1 and CC2, were tested with a concentric axial load; two very similar stress-strain curves were obtained; thus other tests for evaluation of the stress-strain curve of the unreinforced concrete were judged unnecessary for material characterization and the parameters of the stress-strain relationship were tuned on the basis of these results.
The analytical model formulated to reproduce the experimental results uses the unconfined and confined concrete stress-strain relationship proposed by Saatcioglu and Razvi (1992), while for the steel of the reinforcing bars a bilinear model able to take into account hardening in tension and post-buckling behaviour in compression (Dhakal and Maekawa, 2002) is assumed.
The concrete constitutive law was chosen due to its reliability as shown in experimental tests on specimens subjected to an eccentric axial load (Saatcioglu *et al.*, 1995, Campione *et al.*, 2010). The model for reinforcing steel bars proposed by Dhakal and Maekawa (2002) was validated by the results of several experimental tests reported by the authors themselves, and was also chosen taking into account its straightforwardness.
The concrete stress-strian relationship consists in two branches:

$$\tilde{f}_c = \left(2\,\tilde{\varepsilon} - \tilde{\varepsilon}^2\right)^{\beta} \qquad 0 \le \tilde{\varepsilon} \le 1 \tag{3.1}$$

$$\tilde{f}_c = 1 + \tilde{E}\,(\tilde{\varepsilon} - 1) \qquad 1 \le \tilde{\varepsilon} \le \mu_c \tag{3.2}$$

where superscript "~" denotes stress and strains normalized with respect to peak strength and corresponding strain respectively, and μ_c the available ductility, which is defined as the ratio between the ultimate specific strain and the strain corresponding to the peak strength. The elasticity modulus appearing in Eqn. 3.2 is the modulus that describes the negative slope of the softening branch; it has been made dimensionless with respect to the secant modulus. For confined concrete, the following values of the numerical parameters were tuned according to the experimental tests: confined concrete strength f_{cco}=34.34 MPa, corresponding strain ε_{cco}=0.00616, β=0.559, and $\tilde{E} = -0.0729$. The maximum available ductility was assumed equal to 4. For unconfined concrete placed outside the core, the strength and strain are those deduced by the aforementioned experimental tests on cylindrical specimens, while the modulus $\tilde{E}$ is deduced according to the value ε_{co85}.

Referring to the tensile reinforcement, the linear relationship that reproduces the tensile hardening behaviour is modelled by assuming a hardening modulus equal to 1% of the elasticity modulus, while the post-yielding branch of the compressed reinforcement, according to the Dhakal and Maekawa (2002) model, is still characterized by a positive slope reduced to 0.45% of the elasticity modulus.

Fig. 3.1a) shows the experimental test results obtained and the specimen responses modelled on the basis of the stress-strain laws adopted. The analytical curves are interrupted at the first collapse of stirrups for the CC1 specimen. The configuration of the specimen at the end of the tests is shown in Fig. 3.1b).

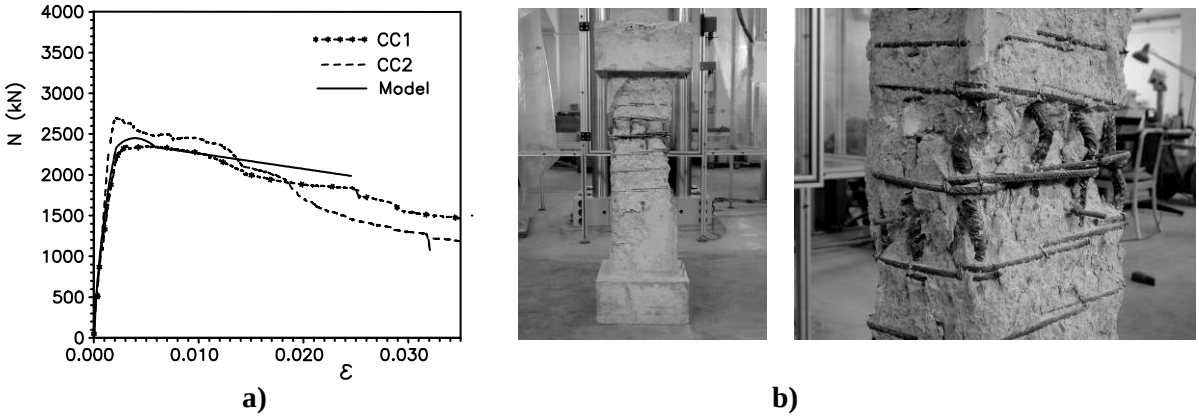

Figure 3.1. a) Experimental and analytical results b) Specimen CC1 after test

4. AXIAL LOAD AND UNIAXIAL BENDING

For the tests under axial action and uni-axial bending analytical expressions of the strength domain at yielding and at ultimate condition were deduced. The formulation is based on the following assumptions: *i*) the resisting section consists of the confined core, delimited by the perimeter corresponding to the stirrup axis; *ii*) the reinforcements contained by the corner reinforcing bars parallel to the plane where the bending moment acts are uniformly distributed along a segment having length equal to $d_1 = s\,(n_b+1)$ where s is the distance between two adjacent bass and n_b is the number of bars along each side; *iii*) collapse is reached when the ultimate concrete strain is overcome; *iv)* after the yielding phase, the tensile and compressed reinforcement have the same behaviour. The latter assumption can be removed with suitable modification of the relationship deduced. However, it was

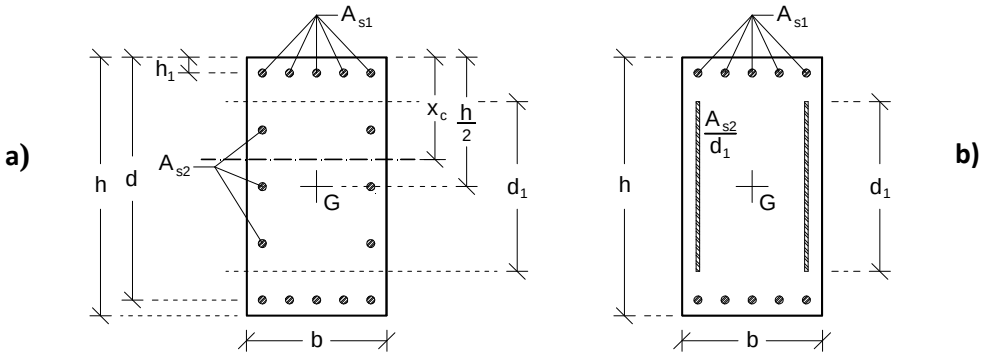

Figure 4.1. a) Actual section scheme; b) Model of section for bending moment acting in vertical plane

retained for the specimens considered here since the small spacing of the stirrups also enables the compressed reinforcements to have hardening behavior in a large strain range, even if a smaller residual elasticity modulus with respect to that in tension is exhibited.
The model scheme and the symbols utilized are shown in Fig.4.1. For brevity's sake, details of the model derivation are not shown, while the analytical expression deduced are given below.
At first yielding of the reinforcement the following relations hold:

$$n=\frac{S_{1,\tilde{\varepsilon}_c}}{\tilde{\varphi}_y}+\omega\left(\frac{\tilde{\varphi}_y}{\tilde{\varphi}_{y,sym}}-1\right)$$

$$m_y=m_{cy}+\frac{\tilde{\varphi}_y}{\tilde{\varepsilon}_{sy}}\left[\omega_1\left(\frac{1-2\lambda}{2}\right)^2+\omega_2\frac{\alpha^2}{12}\right] \qquad \tilde{\varphi}_y \le \tilde{\varphi}_{y,sym} \qquad (4.1)$$

$$n=\frac{S_{1,\tilde{\varepsilon}_c}}{\tilde{\varphi}_y}+\left(\omega_1\tilde{E}_h+\omega_2\right)\left(\frac{\tilde{\varphi}_y}{\tilde{\varphi}_{y,sym}}-1\right)$$

$$m_y=m_{cy}+\omega_1\frac{1-2\lambda}{2}\left[1+\tilde{E}_h\left(\frac{\tilde{\varphi}_y}{\tilde{\varphi}_{y,sym}}-1\right)\right]+\omega_2\frac{\tilde{\varphi}_y}{\tilde{\varepsilon}_{sy}}\frac{\alpha^2}{12} \qquad \tilde{\varphi}_{y,sym} \le \tilde{\varphi}_y \le \tilde{\varphi}_{y,2-3} \qquad (4.2)$$

$$n=\frac{S_{1,\tilde{\varepsilon}_c}}{\tilde{\varphi}_y}+\left(\omega_1\tilde{E}_h+\omega_2\right)\left(\frac{\tilde{\varphi}_y}{\tilde{\varphi}_{y,sym}}-1\right)-2\,\overline{\omega}_2\,(1-\tilde{E}_h)\frac{\tilde{\varepsilon}_{sy}}{\tilde{\varphi}_y}\left(\frac{\tilde{\varphi}_y}{\tilde{\varphi}_{y,2-3}}-1\right)^2$$

$$m_y=m_{cy}+\omega_1\frac{1-2\lambda}{2}\left[1+\tilde{E}_h\left(\frac{\tilde{\varphi}_y}{\tilde{\varphi}_{y,sym}}-1\right)\right]+\omega_2\frac{\tilde{\varphi}_y}{\tilde{\varepsilon}_{sy}}\frac{\alpha^2}{12}+ \qquad \tilde{\varphi}_{y,2-3} \le \tilde{\varphi}_y \qquad (4.3)$$

$$-\frac{2}{3}\overline{\omega}_2\left(1-\tilde{E}_h\right)\left(\frac{\tilde{\varphi}_y}{\tilde{\varphi}_{y,2-3}}-1\right)^2\left(\frac{2\,\overline{\varepsilon}_{sy}}{\tilde{\varphi}_y}+\alpha-\frac{1-2\lambda}{2}\right)\frac{\tilde{\varepsilon}_{sy}}{\tilde{\varphi}_y}$$

While at ultimate yielding the corresponding values are:

$$n = \frac{S_{1,\mu_c}}{\tilde{\varphi}_u} + (2\mu_c - \tilde{\varphi}_u)\left[\frac{\tilde{E}_h}{2\tilde{\varepsilon}_{sy}}\omega + \frac{\overline{\omega}_2}{\tilde{\varphi}_u}(1-\tilde{E}_h)\right]$$

$$m_u = \frac{S_{1,\mu_c}}{2\tilde{\varphi}_u^2}\left[2\tilde{\varepsilon}_{G,\mu_c} - (2\mu_c - \tilde{\varphi}_u)\right] + \frac{\tilde{E}_h}{\tilde{\varepsilon}_{sy}}\left[\omega_1\frac{(1-2\lambda)^2}{4} + \frac{\alpha^2}{12}\omega_2\right]\tilde{\varphi}_u + \tag{4.4}$$

$$+(1-\tilde{E}_h)\left\{\omega_1\frac{1-2\lambda}{2} + \overline{\omega}_2\left[\frac{\alpha^2}{4} - \frac{\tilde{\varepsilon}_{sy}^2}{3\tilde{\varphi}_u^2} - \frac{1}{4\tilde{\varphi}_u^2}(2\mu_c - \tilde{\varphi}_u)^2\right]\right\}$$

The symbols appearing in the previously shown relationship express the following non-dimensionless quantities:

$$n = \frac{N}{b\,h\,f_{cco}} \qquad m_y = \frac{M_y}{b\,h^2\,f_{cco}} \qquad m_u = \frac{M_u}{b\,h^2\,f_{cco}} \tag{4.5}$$

$$\omega_1 = \frac{2\,A_{s1}\,f_{sy}}{b\,h\,f_{cco}} \qquad \omega_2 = \frac{2\,A_{s2}\,f_{sy}}{b\,h\,f_{cco}} \qquad \overline{\omega}_2 = \frac{\omega_2}{\alpha} \qquad \omega = \omega_1 + \omega_2 \tag{4.6}$$

$$\alpha = \frac{d_1}{h} \qquad \tilde{\varphi}_y = \frac{\varphi_y h}{\varepsilon_{cco}} \qquad \tilde{\varphi}_u = \frac{\varphi_u h}{\varepsilon_{cco}} \tag{4.7}$$

$$\lambda = \frac{h_1}{h} \qquad \tilde{\varphi}_{y,sym} = \frac{2\tilde{\varepsilon}_{sy}}{1-2\lambda} \quad \tilde{\varphi}_{y,2-3} = \frac{4\tilde{\varepsilon}_{sy}}{\alpha+1-2\lambda} \tag{4.9}$$

where $\tilde{\varepsilon}_{sy}$ is the reinforcement yielding strain made dimensionless with respect to ε_{cco} and $\tilde{E}_h$ the hardening axial modulus of the reinforcing bar, made dimensionless with respect to the elastic modulus.
Moreover, the following notations are introduced:

$$S_{1,\tilde{\varepsilon}_c} = \int_0^{\tilde{\varepsilon}_c} \tilde{f}_c(\tilde{\varepsilon})\,d\tilde{\varepsilon} \qquad S_{2,\tilde{\varepsilon}_c} = \int_0^{\tilde{\varepsilon}_c} \tilde{f}_c(\tilde{\varepsilon})\,\tilde{\varepsilon}\,d\tilde{\varepsilon} \tag{4.10}$$

$$\tilde{\varepsilon}_{G,\tilde{\varepsilon}_c} = \frac{S_{2,\tilde{\varepsilon}_c}}{S_{1,\tilde{\varepsilon}_c}} \qquad m_{cy} = \frac{S_{1,\tilde{\varepsilon}_c}}{\tilde{\varphi}_y^2}\left[\tilde{\varepsilon}_G + \tilde{\varepsilon}_{sy}\left(1 - \frac{\tilde{\varphi}_y}{\tilde{\varphi}_{y,sym}}\right)\right] \tag{4.11}$$

The minimum and maximum values of the ultimate curvature that define the admissibility range of Eqs. (4.4) are derived by imposing the condition that the lower and upper fibres of the internal uniformly distributed secondary reinforcement are at the first yielding.
For every given value of $\tilde{\varphi}_y$, Eqs. (4.1), (4.2), and (4.3) provide the couple of values n, m_y allowing one to draw the section yielding surface. An analogous procedure can be adopted in order to derive the ultimate surface by using Eq. (4.4)
With reference to the specimen section tested and considering the direction of the maximum inertia, the yielding and ultimate surface shown in Fig. 4.2a) are obtained. The axial load values of N=300 kN and N=1248 kN highlighted in the figure correspond to a generic small axial load and to the greatest value of axial load recorded during the two experimental tests performed, which are described below. In the first case the ultimate moment is greater than the yielding one, while in the second case (high axial compression level) the opposite condition occurs and the ultimate moment is greater than the yielding counterpart.
The effectiveness of the proposed analytical procedure is proved by comparison of these results with the results in Figs. 4.2b) and 4.2c), where for the aforementioned N values of the section moment vs.

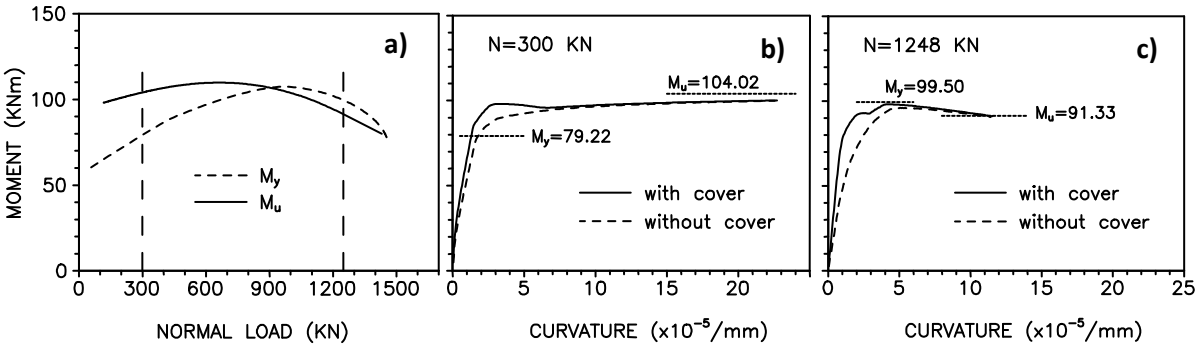

Figure 4.2. a) *M-N* domains (analytical); b) and c) *M-φ* curves for given *N* (numerical)

curvature curves are shown; they are derived by a numerical procedure, using the discretized fibre model taking into account the actual position of the secondary reinforcing bars. The results were derived both by modelling and neglecting the unconfined concrete outside the inner core (which have been neglected in the analytical model). The ultimate and yielding moments shown in Figs. 4.2b) and 4.2c) are evaluated by the analytical procedure and can be compared with the corresponding ones on the curves in Fig. 4.2a). The results prove the great precision of the proposed closed-form expressions.

In the experimental tests with constant eccentricity of the axial load two specimens, denoted with the labels CEY1 and CEY2 (Y is the eccentricity direction), were tested by applying the axial load on the principal central axis parallel to the long side of the section, and two with eccentricity parallel to the short side, namely specimens CEX1 and CEX2. Namely, a load eccentricity e=66 mm corresponding to the ratio e/h =0.22 and e =55 mm corresponding to e/h =0.25 respectively were assumed.

The results of the experimental test for specimens CEY1 and CEY2 are shown in Fig. 4.3: The abscissa in graph 4.3a) is the displacement of the press plate, which was imposed with a load rate of 0.2 mm/min, and the ordinate is the monitored axial load. The peak values of the curves in Fig. 4.3a) are 1248 kN and 1416 kN respectively.

The curves in Fig. 4.3b) confirm the reliability of both the numerical model and the analytical formulation. The numerical curves were derived according to two different procedures. In the first one the maximum value of the axial load was evaluated that corresponded to the eccentricity value obtained as the sum of that imposed at the specimen top and bottom ends and that produced at the specimen mid-height section by the lateral specimen displacement (P-Δ effect); the latter was evaluated by assuming a constant curvature along all the height of the specimen. The second curve was deduced by an analogous procedure, by imposing the yielding condition for the tensile reinforcement farthest from the neutral axis. The analytical curve was evaluated using Eqs. (4.1), or (4.2) or (4.3) depending on the curvature value considered.

Comparison of the analytical and numerical curves confirms the effectiveness of the proposed model: the simplification on the behaviour of the compressed reinforcement introduced in the analytical model only produces appreciable differences for larger eccentricity values, the latter corresponding to the greater values of the curvature.

Comparison between the numerical curves obtained without imposing the reinforcement yielding condition and the analytical and numerical ones obtained by imposing the yielding condition shows that, when eccentricity values slightly larger than $h/6$ occur (50 mm in this case), the maximum load that the section is able to withstand is very similar to that produced by first yielding for tensile reinforcement.

Fig.4.4 shows the picture of specimen CEY2 at the end of the test, where one can easily recognize the rupture of the concrete cover and the buckling of the compressed longitudinal reinforcement, and consequent progressive lack of confinement action by the stirrups.

A similar consideration can be made for the two specimens CEX1 and CEX2; the results relating to them are shown in Fig. 4.5. The pictures in Fig.4.6 show the most damaged part of specimen CEX1 at the end of the test and the device placed at the top and the base of the specimens, together with the rotation at the end of the test undergone by the specimen.

.

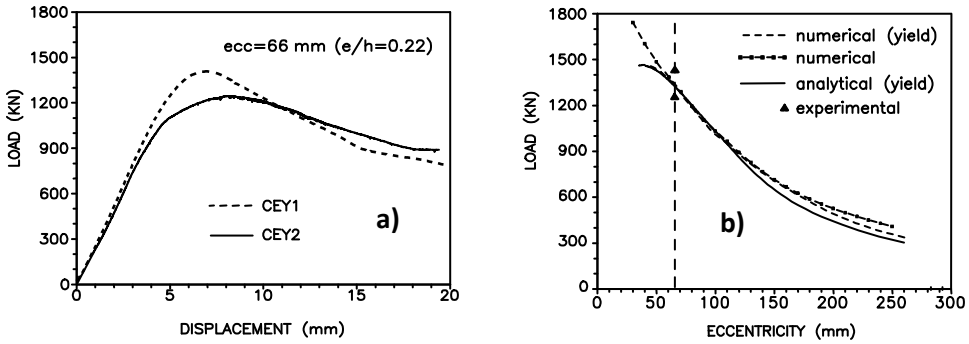

Figure 4.3. a) Experimental results; b) Analytical and numerical modelling

Figure 4.4. Specimen CEY2 after test

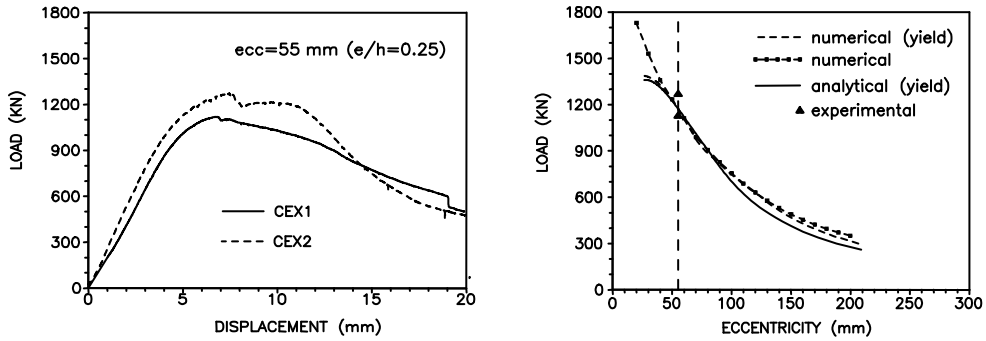

Figure 4.5. Experimental, numerical and analytical results of specimens CEX1 and CEX2

Figure 4.6. Ultimate state of specimen CEX1; rotation of device at the top and base of specimens

5. AXIAL LOAD AND BIAXIAL BENDING

Two specimens, namely CEXY1 and CEXY, were tested by imposing an axial load with eccentricity equal to 33 mm in the *x* direction (short side of the section) and 70 mm in the *y* direction. These values were chosen in order to be consistent with the features of the test setup so as to produce flexure with the neutral axis with an inclination of 45° degrees in the section plane, according to a preliminary evaluation of the response by the numerical procedure. This setup allows one to transfer the load to the specimens along the generatrix of the steel cylinder interposed between the press cylinders and the specimen ends, rotating the device itself 45 degrees in the section plane.
In order to avoid premature collapse of the specimen end regions, for this type of test the base and top parts of the specimen were preliminarily reinforced by steel jackets made up of four angles at the corners and two plates for each side.
The curves of the axial load vs. the relative displacement of the press cylinders recorded during the test are shown in Fig. 5.1a), where the maximum values of the load are also reported. The two specimens exhibit similar behavior. As expected, the reinforcement cover was subjected to more extensive damage with respect to the case of flexure along one of the principal axes; this circumstance was also stressed in Zahn *et al.* (1989). In both cases the collapse was due to stirrup collapse after buckling of the corner reinforcing bar in compression, followed by the same behaviour for the nearest reinforcing bars.
For this loading condition, only numerical model were developed, using the fibre model previously mentioned and determining the relations between the bending moment components in the two directions by assuming a constant level of the axial load equal to the maximum value recorded in the two tests. The analysis was performed imposing an ultimate condition corresponding to the attainment of ultimate deformation in the compressed confined concrete and a yielding condition corresponding to the first yielding of the tensile reinforcing bar, by varying the inclination of the neutral axis. The results of the analysis are shown in Fig. 5.1b), where the notation "X-X" and "Y-Y" denotes respectively the components of the moment vector along the section horizontal and vertical axes, namely those obtained by the product of the axial load times eccentricity in the *x* and *y* directions.
The results confirm the observations deduced for the case of uniaxial bending moment, namely the observation that for the assumed values of the load eccentricity, to the maximum axial load there corresponds a bending moment value comprised between those at the yielding and collapse conditions. Fig. 5.1c) shows the specimen CEXY1 at the end of the test.

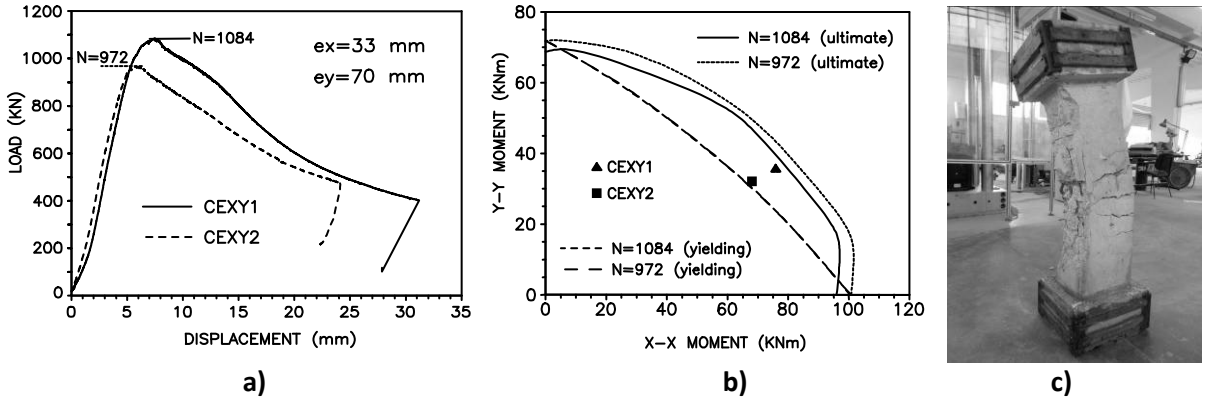

Figure 5.1. a) Experimental results; b) Comparison with numerical results; c) Specimen CEXY1 during test

ACKNOWLEDGEMENT
This work was carried out within the 2010-2013 Research Project "DPC–ReLUIS (Dipartimento Protezione Civile - Rete dei Laboratori Universitari di Ingegneria Sismica)", AT 1, Task 1.1.2. The related financial support was greatly appreciated.

REFERENCES

ACI 318. Building code requirements for structural concrete and commentary. American Concrete Institute (ACI); 2008.

Eurocode 2. Design of concrete structures, Part 1-1: general rules and rules for buildings. European Committee for Standardization (CEN); 2005.

Mari, A.R. and Scordelis, A.C. (1973). Nonlinear geometric, material and time dependent analysis of three dimensional reinforced and prestressed concrete frames. USB/SESM Rep. 84/12, Department of Civil Engineering, University of California, Berkeley, USA.

Bonet, J., Miguel, P.F., Fernandez, M.A. and Romero, M.L. (2001). Efficient procedure for stress integration in concrete sections using a Gauss-Legendre cuadrature. *Eighth International Conference on Civil and Structural Engineering Computing*, Paper 53.

Fafitis, A. (2001). Interaction surfaces of reinforced-concrete sections in biaxial bending. *Journal of Structural Engineering (ASCE)* **127:7**,840-846.

Di Ludovico, M., Lignola, G.P., Prota, A. and Cosenza, E. (2010). Nonlinear analysis of cross-sections under axial load and biaxial bending. *ACI Structural Journal* **107:4**, 390-399.

Bresler, B. (1960). Design criteria for reinforced columns under axial load and biaxial bending. *ACI Journal* **57: 5**:481-490.

Bonet, J., Miguel, P.F., Fernandez, M.A. and Romero, M.L. (2004). Analytical approach to failure surfaces in reinforced concrete sections subjected to axial loads and biaxial bending. *Journal of Structural Engineering (ASCE)* **130:12**,2006-2015.

Monti, G. and Alessandri, S. (2006). Assessment of rc columns under combined biaxial bending and axial load. *Second FIB Congress*. Paper 10-8.

Zahn, F.A., Park, R. and Priesley, N.J. (1989). Strength and ductility of square reinforced concrete column sections subjected to biaxial bending. *ACI Structural Journal* **56:2**, 123-131.

Bahn, B.Y. and Hsu, C.T. (2000). Cyclically and biaxially loaded reinforced concrete slender columns. *ACI Structural Journal* **97:3**, 444-454.

Rammamurthy, L.N. (1966). Investigation of the ultimate strength of square and rectangular columns under biaxial eccentric loads. *Reinforced Concrete Columns, SP-13 (ACI)*, 263-298.

Saatcioglu, M. and Razvi, S.R. (1992). Strength and ductility of confined concrete. *Journal of Structural Engineering (ASCE)* **118:6**,1590-1607.

Dhakal, R.P. and Maekawa, K. (2002). Modeling for postyield buckling of reinforcement. *Journal of Structural Engineering (ASCE)* **128:9**,1139-1147.

Saatcioglu, M., Salamat, A.H. and Razvi, S.R. (1995). Confined columns under eccentric loading. *Journal of Structural Engineering (ASCE)* **121:11**,1547-1555.

Campione, G., Fossetti, M. and Papia, M. (2010). Behavior of fiber-reinforced concrete columns under axially and eccentrically compressive loads. *ACI Structural Journal* **107:3**,272-281.